MEaSUREs BedMachine Antarctica, Version 3

USER GUIDE

How to Cite These Data

As a condition of using these data, you must include a citation:

Morlighem, M. 2022. *MEaSUREs BedMachine Antarctica, Version 3*. [Indicate subset used]. Boulder, Colorado USA. NASA National Snow and Ice Data Center Distributed Active Archive Center. https://doi.org/10.5067/FPSU0V1MWUB6. [Date Accessed].

We also request that you acknowledge the author(s) of this data set by referencing the following peer-reviewed publication:

Morlighem, M., E. Rignot, T. Binder, D. D. Blankenship, R. Drews, G. Eagles, O., et al. 2020. Deep glacial troughs and stabilizing ridges unveiled beneath the margins of the Antarctic ice sheet, Nature Geoscience. 13. 132-137. https://doi.org/10.1038/s41561-019-0510-8

FOR QUESTIONS ABOUT THESE DATA, CONTACT NSIDC@NSIDC.ORG

FOR CURRENT INFORMATION, VISIT https://nsidc.org/data/NSIDC-0756

National Snow and Ice Data Center

TABLE OF CONTENTS

1 DATA DESCRIPTION

1.1 Parameters

This data set contains a bed topography/bathymetry map of Antarctica deduced by subtracting the ice thickness from the surface elevation taken from the Reference Elevation Model of Antarctica (REMA). Ice thickness is derived via mass conservation, streamline diffusion, and other methods. Ice thicknesss and ice surface elevations are reported in ice equivalent (heights above mean sea level using the EIGEN-6C4 geoid) to account for firn air content.

Additional parameters include errors in the ice thicknesses/bed estimates; the firn correction parameter; geoid height difference from the WGS84 ellipsoid; and an ice/ocean/land mask. A source map is also provided that shows where each method was applied.

1.2 File Information

1.2.1 Format

A single netCDF-4 file, CF-1.7 compliant.

1.2.2 File Contents

All parameters included in the data file are described in Table 1 below:

Table 1. File Parameters and Units

Parameter Name	Description	Units	Valid Values	Type
bed	Bed topography (elevation)	meters	-9000 – 5000	float
dataid	Input data source ID. No data (0); REMA (1); radar (2); seismic (7); multibeam (10).	N/A	0, 1, 2, 7, 10	byte
errbed	Bed topography (ice thickness) error	meters	0 – 1000	short
firn	Firn air content	meters	0 – 50	float
geoid	Geoid height difference from WGS 84 ellipsoid*	meters	-80 – 80	short
mapping	Mapping attributes	N/A	N/A	char
mask	Ocean/ice/land mask: ocean (0); ice-free land (1); grounded ice (2); floating ice (3); Lake Vostok (4).	N/A	0 – 4	byte

Parameter Name	Description	Units	Valid Values	Type
source	Output data source (i.e., method): REMA/IBCSO V2 (1); mass conservation (2); interpolation (3); hydrostatic (4); streamline diffusion (5); gravity (6); seismic (7); multibeam (10).	N/A	1 – 10	byte
surface	Ice surface elevation	meters	0 – 5000	float
thickness	Ice thickness	meters	0 – 5000	float
x	Projection x coordinate	meters	-3333000 – 3333001	int
y	Projection y coordinate	meters	-3333000 – 3333001	int

* To obtain height above the WGS84 ellipsoid, simply add the value of the geoid parameter to the bed parameter.

The following figure is an example of how the bed topography and ice thickness can be viewed as maps:

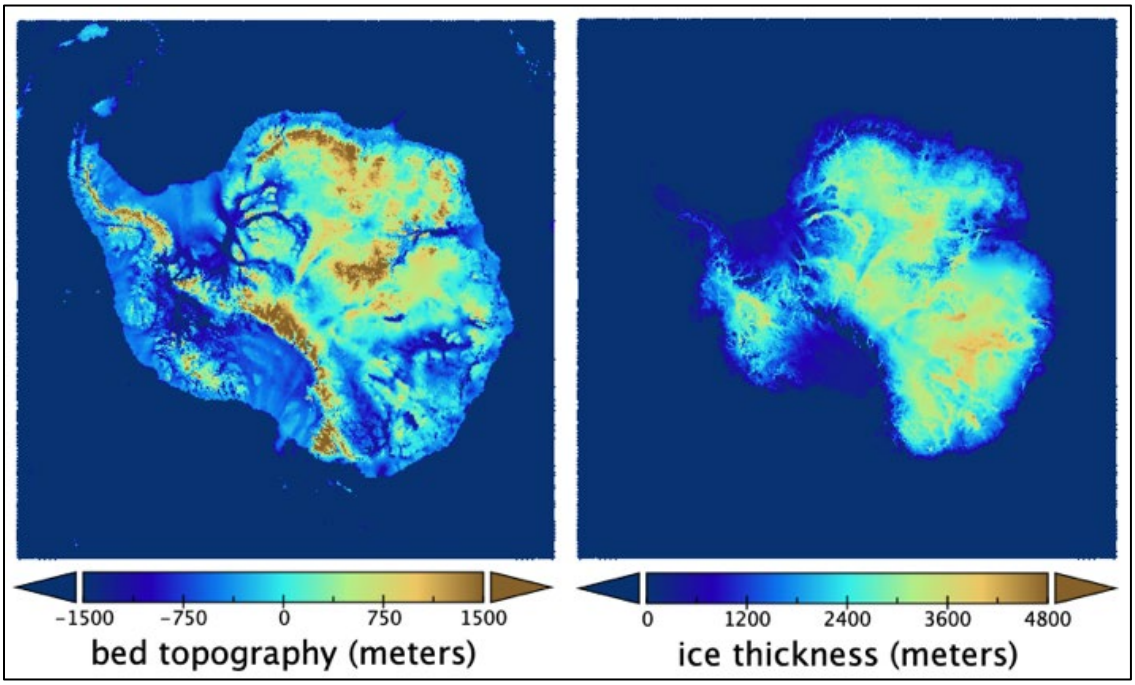

Figure 1. Maps of bed topography (left) and ice thickness (right) created with the Panoply Data Viewer.

1.2.3 Naming Convention

The data file is named BedMachineAntarctica-v3.nc. “v3” indicates this is the Version 3 product.

1.3 Spatial Information

1.3.1 Coverage

Antarctic polar region south of 70º S.

1.3.2 Resolution

500 m

1.3.3 Geolocation

Table 2 provides information for geolocating this data set:

Table 2. Geolocation Details

Geographic coordinate system	WGS 84
Projected coordinate system	WGS 84 / Antarctic Polar Stereographic
Longitude of true origin	0º E
Latitude of true origin	71º S
Scale factor at longitude of true origin	1
Datum	WGS 84
Ellipsoid/spheroid	WGS 84
Units	meter
False easting	0
False northing	0
EPSG code	3031
PROJ4 string	+proj=stere +lat_0=-90 +lat_ts=-71 +lon_0=0 +k=1 +x_0=0 +y_0=0 +datum=WGS84 +units=m +no_defs
Reference	https://epsg.io/3031

1.4 Temporal Information

1.4.1 Coverage

The data were collected between 01 January 1970 and 01 October 2019. The nominal year of this data set is 2015—the year of the reference surface digital elevation model.

2 DATA ACQUISITION AND PROCESSING

2.1 Input Data

This data set was generated from the following input data:

- Ice thickness from 1967 to 2020 obtained by 47 airborne ice penetrating radar survey campaigns (see Figure 2). Additional sources of ice thickness data include:
    - CReSIS* 2018, CReSIS 2019
    - British Antarctic Survey Polarimetric radar Airborne Science Instrument (PASIN) data
    - Young et al. (2017) and Cui et al. (2020), to constrain bed topography under grounded ice
    - Smith et al. (2020) for thinning rates
- Ice flow velocity derived from satellite interferometry (Rignot et al., 2011; Mouginot et al., 2017)
- Surface mass balance obtained with a regional atmospheric climate model (RACMO2; van Wessem et al., 2018), representative of the period 1961-1990
- Surface topography from the Reference Elevation Model of Antarctica (REMA; Howat et al., 2019)
- The International Bathymetric Chart of the Southern Ocean (IBCSO), V2
- Multi-beam ocean bathymetry data in the Amundsen Sea embayment (Hogan et al., 2020) as well as gravity inversions for this sector (Jordan et al., 2020).

*The Center for Remote Sensing and Integrated Systems. For more information about CReSIS Antarctic campaigns, see CReSIS in Antarctica.

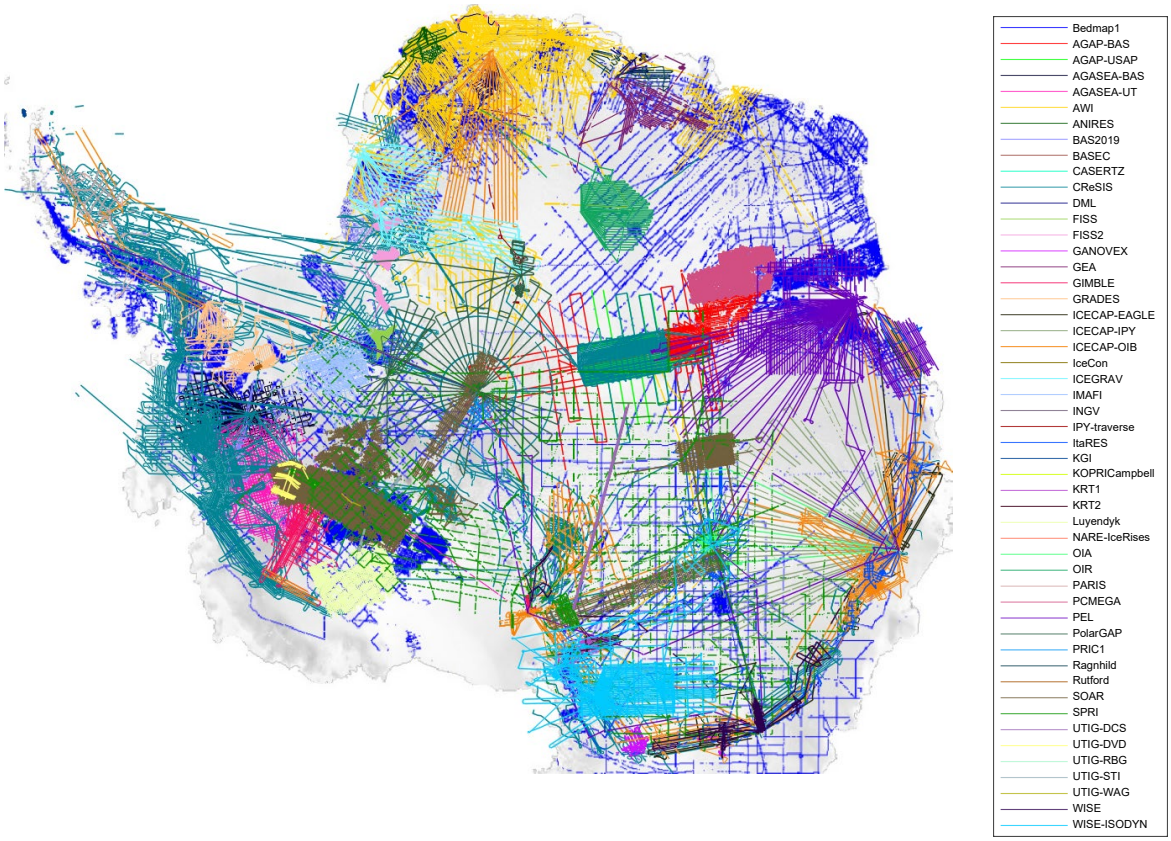

Figure 2. Ice thicknesses were in large part derived from 47 airborne ice penetrating radar survey campaigns flown between 1967 and 2020. References and the institutions involved in each campaign (plotted above) are available in Table S1 in Morlighem et al. (2020).

2.2 Ice Thickness Mapping

Different methods were used to map ice thickness depending on the ice characteristics: mass conservation in regions of fast-moving ice; streamline diffusion in regions of slow-moving ice; hydrostatic equilibrium for floating ice shelves; and gravity inversion and seismic bathymetry for grounded ice shelves.

The mass conservation (MC) method yields ice thickness and bed topography that compares favorably with ice sheet numerical models; resolves uncertainties in previous estimates interpreted from radar echoes; and ensures that grounding line fluxes are compatible with snowfall accumulation and thinning rates in the interior, without assuming steady-state.

Ice surface motion offers a physical basis to extrapolate sparse ice thickness data to larger areas with little or no data. The method works best in areas of fast flow (ice surface velocity > 30 m/yr) where errors in flow direction are small and the glaciers slide on the bed.

The MC method combines sparse, airborne, radar-sounding-derived ice thickness data with high-resolution ice motion derived from satellite interferometric synthetic-aperture radar and mass balance to estimate ice thickness across the entire continent. The algorithm conserves mass fluxes while minimizing the departure from the original radar-derived ice thickness data. The mathematical formulae of this method are summarized in Morlighem et al. (2019, Supplementary Information) and extensively detailed in Morlighem et al. (2011, 2014, 2017).

In the interior slow-moving sectors, where errors in flow direction are larger, streamline diffusion is used to interpolate ice thickness. This approach was chosen as an alternative to more commonly used methods, such as kriging or splines, because it better captured the intrinsic anisotropy of the ice thickness that mass conservation requires — namely, that as ice is transported downstream, ice thickness varies slowly along the flow. Across flow, significantly higher gradients in ice thickness are expected. The diffusion equation accounts for this asymmetry. While not based on physics, it is a way to interpolate ice thickness anisotropically between flight lines. See Morlighem et al. (2019, Supplementary Information) for more details.

On floating ice shelves, hydrostatic equilibrium is applied with a calibrated firn depth correction so the inferred ice thickness is consistent with available ice shelf thickness data, thus ensuring continuity in ice thickness across the grounding line.

Individual MC ice thickness maps are constrained by flight lines along their boundaries. All the MC maps are stitched together using simple interpolation (inverse distance weighting), and combined with the ice thickness maps derived via streamline diffusion. The Antarctic bed topography is derived by subtracting the resulting ice thickness map from the REMA surface digital elevation model (Howat et al., 2019). Over ice-free land areas, the bed topography is the REMA itself.

2.2.1 Firn Air Correction

The surface elevation and ice thickness maps provided in this data set are given in ice equivalent, as they include the firn air content correction (i.e., they are lower than they would be if the air column height was included). The elevation of the top of the snow as provided by REMA can be reconstructed by adding the firn depth correction (firn air content) to the ice surface elevation provided in the data file:

$$S_{REMA} = S_{BedMachine} + d_{firn}$$

2.3 Data Quality and Errors

Error estimates of the bed elevation and ice thickness are provided in the data set. Sources of error include error in ice velocity direction and magnitude, error in surface mass balance, and ice thinning rates.

In a trial setting with unusually dense radar sounding coverage, errors in the MC-inferred thickness are reported at 36 m, only slightly higher than that of the original data. In areas less well constrained by radar-derived thickness data, or constrained by only one track of data (e.g., in East Antarctica), errors may exceed 200 m (Morlighem et al., 2020). And in areas where sparse ice shelf bathymetry are available, uncertainty may exceed 500 m.

3 SOFTWARE AND TOOLS

See NetCDF Resources at NSIDC: Software and Tools.

4 VERSION HISTORY

Table 3. Version History Summary

Version	Release Date	Description of Changes
V3	October 2022	Changes for Version 3 include: • Added ice thickness measurements from CReSIS 2018, CReSIS 2019, and PASIN • Updated thinning rates per Smith et al. (2020) • Added parameter (“dataid”) to more easily identify data source • Uses IBCSO v2 for ocean bathymetry
V2	September 2020	Changes to this version include: • Additional thickness data to constrain the bed topography under grounded ice • New multi-beam bathymetry data, as well as gravity inversions, integrated in the Amundsen Sea embayment • An error in geoid height was corrected for the IBCSO bathymetry
V1	December 2019	Initial release

5 RELATED DATA SETS

IceBridge BedMachine Greenland

6 RELATED WEBSITES

NASA MEaSUREs Data at NSIDC

NASA MEaSUREs

Antarctic Ice Sheet Velocity (AIV) and Mapping Data at NSIDC

7 CONTACTS AND ACKNOWLEDGMENTS

Mathieu Morlighem
University of California Irvine

8 REFERENCES

Arndt, J. E., Schenke, H. W., Jakobsson, M., Nitsche, F. O., Buys, G., Goleby, B., et al. (2013). The International Bathymetric Chart of the Southern Ocean (IBCSO) Version 1.0-A new bathymetric compilation covering circum-Antarctic waters. Geophysical Research Letters, 40(12), 3111–3117. https://doi.org/10.1002/grl.50413

Cui, X., Jeofry, H., Greenbaum, J. S., Guo, J., Li, L., Lindzey, L. E., Habbal, F. A., Wei, W., Young, D. A., Ross, N., Morlighem, M., Jong, L. M., Roberts, J. L., Blankenship, D. D., Bo, S., & Siegert, M. J. (2020). Bed topography of Princess Elizabeth Land in East Antarctica. Copernicus GmbH. https://doi.org/10.5194/essd-2020-126

Greenbaum, J. S., Blankenship, D. D., Young, D. A., Richter, T. G., Roberts, J. L., Aitken, A. R. A., et al. (2015). Ocean access to a cavity beneath Totten Glacier in East Antarctica. Nature Geoscience, 8(4), 294–298. https://doi.org/10.1038/ngeo2388

Hogan, K. A., Larter, R. D., Graham, A. G. C., Arthern, R., Kirkham, J. D., Totten Minzoni, R., Jordan, T. A., Clark, R., Fitzgerald, V., Wåhlin, A. K., Anderson, J. B., Hillenbrand, C.-D., Nitsche, F. O., Simkins, L., Smith, J. A., Gohl, K., Arndt, J. E., Hong, J., & Wellner, J. (2020). Revealing the former bed of Thwaites Glacier using sea-floor bathymetry: implications for warm-water routing and bed controls on ice flow and buttressing. The Cryosphere, 14(9), 2883–2908. https://doi.org/10.5194/tc-14-2883-2020

Howat, I. M., Porter, C., Smith, B. E., Noh, M.-J., & Morin, P. (2019). The Reference Elevation Model of Antarctica. The Cryosphere, 13(2), 665–674. https://doi.org/10.5194/tc-13-665-2019

Jordan, T. A., Porter, D., Tinto, K., Millan, R., Muto, A., Hogan, K., Larter, R. D., Graham, A. G. C., & Paden, J. D. (2020). New gravity-derived bathymetry for the Thwaites, Crosson, and Dotson ice

shelves revealing two ice shelf populations. The Cryosphere, 14(9), 2869–2882. https://doi.org/10.5194/tc-14-2869-2020

Millan, R., Rignot, E., Bernier, V., Morlighem, M., & Dutrieux, P. (2017). Bathymetry of the Amundsen Sea Embayment sector of West Antarctica from Operation IceBridge gravity and other data. Geophysical Research Letters, 44(3), 1360–1368. https://doi.org/10.1002/2016gl072071

Morlighem, M., Rignot, E., Seroussi, H., Larour, E., Ben Dhia, H., & Aubry, D. (2011). A mass conservation approach for mapping glacier ice thickness. Geophysical Research Letters, 38(19), 1-6. https://doi.org/10.1029/2011gl048659

Morlighem, M., Rignot, E., Mouginot, J., Seroussi, H., & Larour, E. (2014). Deeply incised submarine glacial valleys beneath the Greenland ice sheet. Nature Geoscience, 7(6), 418–422. https://doi.org/10.1038/ngeo2167

Morlighem, M., Williams, C. N., Rignot, E., An, L., Arndt, J. E., Bamber, J. L., et al. (2017). BedMachine v3: Complete Bed Topography and Ocean Bathymetry Mapping of Greenland From Multibeam Echo Sounding Combined With Mass Conservation. Geophysical Research Letters, 44(21), 11,051-11,061. https://doi.org/10.1002/2017gl074954

Morlighem, M., Rignot, E., Binder, T., Blankenship, D., Drews, R., Eagles, G., et al. (2020). Deep glacial troughs and stabilizing ridges unveiled beneath the margins of the Antarctic ice sheet. Nature Geoscience, 13, 132–137. https://doi.org/10.1038/s41561-019-0510-8

Mouginot, J., Rignot, E., Scheuchl, B., & Millan, R. (2017). Comprehensive Annual Ice Sheet Velocity Mapping Using Landsat-8, Sentinel-1, and RADARSAT-2 Data. Remote Sensing, 9(4), 364. https://doi.org/10.3390/rs9040364

Rignot, E., Velicogna, I., van den Broeke, M. R., Monaghan, A., & Lenaerts, J. T. M. (2011). Acceleration of the contribution of the Greenland and Antarctic ice sheets to sea level rise. Geophysical Research Letters, 38(5), n/a-n/a. https://doi.org/10.1029/2011gl046583

Rosier, S., H. R., Hofstede, C., Brisbourne, A. M., Hattermann, T., Nicholls, K. W., Davis, P. E. D., et al. (2018). A New Bathymetry for the Southeastern Filchner-Ronne Ice Shelf: Implications for Modern Oceanographic Processes and Glacial History. Journal of Geophysical Research: Oceans, 123(7), 4610–4623. https://doi.org/10.1029/2018jc013982

Smith, B., H.A. Fricker, A.S. Gardner, B. Medley, J. Nilsson, F.S. Paolo, N. Holschuh, S. Adusumilli, K. Brunt, B. Csatho, K. Harbeck, T. Markus, T. Neumann, M.R. Siegfried, H. J. Zwally. 2020. Pervasive ice sheet mass loss reflects competing ocean and atmosphere processes. Science, 368(6496), 1239–1242. https://doi.org/10.1126/science.aaz5845

Tinto, K. J., Padman, L., Siddoway, C. S., Springer, S. R., Fricker, H. A., Das, I., et al. (2019). Ross Ice Shelf response to climate driven by the tectonic imprint on seafloor bathymetry. Nature Geoscience, 12(6), 441–449. https://doi.org/10.1038/s41561-019-0370-2

van Wessem, J. M., van de Berg, W. J., Noël, B. P. Y., van Meijgaard, E., Amory, C., Birnbaum, G., et al. (2018). Modelling the climate and surface mass balance of polar ice sheets using RACMO2 – Part 2: Antarctica (1979–2016). The Cryosphere, 12(4), 1479–1498. https://doi.org/10.5194/tc-12-1479-2018

Young, D. A., Roberts, J. L., Ritz, C., Frezzotti, M., Quartini, E., Cavitte, M. G. P., Tozer, C. R., Steinhage, D., Urbini, S., Corr, H. F. J., van Ommen, T., & Blankenship, D. D. (2017). High-resolution boundary conditions of an old ice target near Dome C, Antarctica. The Cryosphere, 11(4), 1897–1911. https://doi.org/10.5194/tc-11-1897-2017

9 DOCUMENT INFORMATION

9.1 Publication Date

September 2020

9.2 Date Last Updated

October 2022